Progress In Electromagnetics Research, PIER 24, 311–335, 1999

SDRA APPROACH FOR HIGHER-ORDER IMPEDANCE BOUNDARY CONDITIONS FOR COMPLEX MULTI-LAYER COATINGS ON CURVED CONDUCTING BODIES

V. Galdi and I. M. Pinto *

The Waves Group, D.I.I.I.E.
University of Salerno
via Ponte don Melillo
I-84084 Fisciano (SA), Italy

1. INTRODUCTION

Computation of electromagnetic (henceforth EM) fields scattered by surface-treated (e.g., multi-layer coated, corrugated) objects is a key task in many engineering problems such as analysis of radar

* Also with University of Sannio at Benevento, I-82100, Benevento, Italy.

signatures [1], shields [2, 3], absorbers [4, 5], etc. Whenever applicable, approximate Impedance Boundary Conditions (henceforth IBCs) [6, 7] provide an effective tool for solving external (internal) EM boundary value problems, reducing significantly the computational cost and often providing useful design hints.

Loosely speaking, approximate IBCs relate the (tangential and/or normal) electric and magnetic field components (and, possibly, a few derivatives thereof) at the (regular) boundary of the domain of interest through linear equations whose coefficients depend on the local (geometric and/or material) surface properties. Traditional numerical techniques, such as Method of Moments [8] or Finite Element [9], can be thus applied for solving the scattering problem *without* the need of computing the field beyond this surface, with consequent simplification and a considerable reduction in the number of unknowns.

The well-known and pretty simple Leontovich IBC [10], which relates the tangential fields by a complex impedance factor, provides accurate results for thin (on a wavelength scale) and/or significantly lossy dielectric layers. Its tensor generalization [7], also gives fairly accurate results for various polarization-rotating (e.g., corrugated) coatings. More accurate approximations can be obtained, and more general coatings can be modeled, by introducing in the approximate IBCs a suitable number of field derivatives. The resulting Generalized IBCs or Higher-Order IBCs (henceforth HOIBCs) [11–14] have been widely applied during the last decade to a variety of scattering problems involving homogeneous [15, 16] and inhomogeneous [17, 18] dielectric layers, dielectric-filled grooves [19] and multilayer coatings [20–22]. Obviously, in these applications one needs to find a clever trade-off between accuracy and computational ease.

Developing more effective and accurate HOIBCs is still a worthwhile issue, in view of the raising complexity of the coatings typically encountered in EM problems. The latter arises both from constitutive (e.g., stratified, inhomogeneous and/or near-future artificial (bi)anisotropic materials) and geometric (e.g., curvature, corrugation) properties. Developing effective CAD tools consequently demands *systematic* and *reliable* procedures for deriving easily implementable HOIBCs capable of modeling such complex features.

In this connection, the Spectral-Domain-Rational-Approximation (henceforth SDRA) approach proposed by Hoppe and Rahmat-Samii [7] is very attractive, meeting most of the above requirements. It

combines a rigorous, systematic spectral domain method to derive *exact* IBCs, with an accurate rational approximation, allowing an *easy* derivation of the sought HOIBCs for homogeneous (possibly stratified) coatings of arbitrary linear (bianisotropic) materials. As a matter of fact, second-order IBCs are shown to be usually capable of accurately modeling relatively complex coatings. In addition, standard models for corrugation can be easily exploited, and (one-dimensional) curvature effects can be efficiently taken into account using a *locally cylindrical* approximation [7].

Recently, we succeeded in extending the aforementioned approach to handle isotropic-inhomogeneous dielectric layers, for the planar case [23]. In this paper we consider the cylindrical case, which is appropriate to describe (locally) curved surfaces. To this end, we solve the canonical problem of plane-wave incidence on either a radially inhomogeneous dielectric layer or a homogeneous bianisotropic one, laid on a general (i.e., polarization rotating) impedance circular cylinder. Following Hoppe and Rahmat-Samii [7], the obtained *exact* IBCs are approximated by means of low-order rational functions of the transverse wavenumber, which yield the sought HOIBCs after straightforward Fourier transformation to the spatial domain.

Ammari and He [18] worked out *explicit* forms (up to the second-order) of HOIBCs for inhomogeneous thin layers coated on perfectly conducting curved surfaces, by using asymptotic expansions (power series in the layer thickness) of the field and the local curvature. By comparison, the SDRA approach expounded here appears more general (allowing, e.g., a simple treatment of multi-layered coatings including bianisotropic materials) and systematic, and thus better suited for inclusion in CAD tools.

The remainder of the paper is organized as follows. Section 2 contains a brief review of HOIBCs for arbitrary bianisotropic layers and a detailed derivation of HOIBCs for arbitrary isotropic, inhomogeneous dielectric layers on an impedance circular cylinder. In Section 3 the procedure is exploited, yielding second-order IBCs on arbitrary curved surfaces. In Section 4, a number of numerical examples are presented and discussed, in order to validate the proposed method and show its improvement with respect to the *locally planar* approximation. Conclusions follow under Section 5. A body of technical details are collected in the Appendices. A time-harmonic dependence $\exp(i\omega t)$ is implicitly assumed and dropped throughout the paper.

2. SPECTRAL DOMAIN IBCS FOR CYLINDRICAL COATED SURFACES

2.1 Exact IBCs for a Homogeneous Bianisotropic Layer on a Cylinder

We start with a generalized derivation (along the lines sketched in [7]) of the exact IBCs for a circular cylindrical surface at $r = a$ in the (r, ϕ, z) coordinate system, described by given IBCs and coated by a homogeneous bianisotropic layer (see Fig. 1) with (general) constitutive relations [24]:

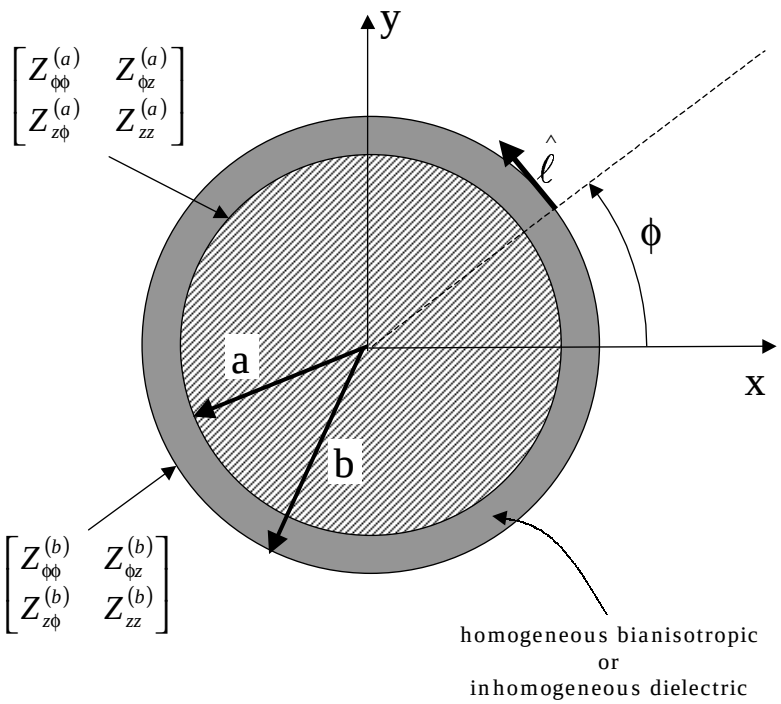

Figure 1. Geometry of canonical problem.

$$\begin{cases} \mathbf{D} = \epsilon_0 \left(\overline{\epsilon} \cdot \mathbf{E} + \eta_0 \overline{\xi} \cdot \mathbf{H} \right), \\ \mathbf{B} = \mu_0 \left(\overline{\mu} \cdot \mathbf{H} + \eta_0^{-1} \overline{\zeta} \cdot \mathbf{E} \right), \end{cases} \tag{1}$$

wherein ϵ_0 and μ_0 are, respectively, the free-space electric permittivity and magnetic permeability, η_0 is the free-space impedance, and

$\overline{\epsilon}$, $\overline{\mu}$, $\overline{\xi}$, $\overline{\zeta}$ are dimensionless 2nd rank tensors.

In order to obtain the sought spectral domain IBCs, we study plane-wave incidence on the coating. We confine ourselves to the case where the incident wave vector is orthogonal to the z axis (normal incidence). Following Hoppe and Rahmat-Samii, the tangential fields (ϕ, z components) in the coating are written as Fourier series [7]:

$$\begin{cases} \mathbf{E}_t(r,\phi) = \displaystyle\sum_{n=-\infty}^{\infty} \hat{\mathbf{E}}_t(n,r)\exp(in\phi) = \sum_{n=-\infty}^{\infty}\sum_{j=1}^{4} c_{jn}\mathbf{e}_t^{(j)}(n,r)\exp(in\phi), \\ \mathbf{H}_t(r,\phi) = \displaystyle\sum_{n=-\infty}^{\infty} \hat{\mathbf{H}}_t(n,r)\exp(in\phi) = \sum_{n=-\infty}^{\infty}\sum_{j=1}^{4} c_{jn}\mathbf{h}_t^{(j)}(n,r)\exp(in\phi), \end{cases} \tag{2}$$

where c_{jn} are unknown coefficients, and $\mathbf{e}_t^{(j)}$, $\mathbf{h}_t^{(j)}$ are the (tangential) *characteristic cylindrical waves* in the medium. These latter can be expressed in terms of the longitudinal components e_z, h_z (Debye potentials) which, in turn, are solutions of two *coupled* Sturm-Liouville problems [25]. These equations are *not* solvable in closed form, in the most general case, and thus numerical or hybrid (e.g., Frobenius [26]) methods should be applied. However, there are some notable exceptions (including, e.g., chiral media [27] and materials where TE-TM decoupling occurs [25]) where *analytical* solutions (possibly in terms of Bessel/Hankel functions) can be readily obtained.

Once the characteristic cylindrical waves have been computed, exact IBCs can be obtained for each value of n, using the orthogonality of the $\exp(in\phi)$ functions, as shown in [7]. As anticipated, the innermost cylinder ($r = a$) is assumed as being described itself by some general tensor IBC:

$$\begin{bmatrix} \hat{E}_\phi(n,a) \\ \hat{E}_z(n,a) \end{bmatrix} = \left[Z^{(a)}(n)\right] \cdot \begin{bmatrix} \hat{H}_\phi(n,a) \\ \hat{H}_z(n,a) \end{bmatrix} = \begin{bmatrix} Z_{\phi\phi}^{(a)}(n) & Z_{\phi z}^{(a)}(n) \\ Z_{z\phi}^{(a)}(n) & Z_{zz}^{(a)}(n) \end{bmatrix} \cdot \begin{bmatrix} \hat{H}_\phi(n,a) \\ \hat{H}_z(n,a) \end{bmatrix}, \tag{3}$$

which can either model the presence of a (possibly lossy, corrugated) metallic surface or represent the effects of *further* layers. This makes extension to stratified coatings immediate, by suitably iterating the procedure.

For each value of n, the four unknown coefficients $c_{1n}, \cdots, c_{4n}$ can be successively eliminated [7] by enforcing the *known* IBCs (3) at $r = a$ and the *sought* IBCs at $r = b$. After some straightforward matrix

algebra one gets:

$$\begin{aligned}\left[Z^{(b)}(n)\right] :&= \begin{bmatrix} Z^{(b)}_{\phi\phi}(n) & Z^{(b)}_{\phi z}(n) \\ Z^{(b)}_{z\phi}(n) & Z^{(b)}_{zz}(n) \end{bmatrix} \\ &= \left([E_{12}(n,b)] + [E_{34}(n,b)] \cdot \left[M^{(a)}(n)\right]\right) \\ &\quad \cdot \left([H_{12}(n,b)] + [H_{34}(n,b)] \cdot \left[M^{(a)}(n)\right]\right)^{-1} \end{aligned} \tag{4}$$

where:

$$\begin{aligned}\left[M^{(a)}(n)\right] &= \left(\left[Z^{(a)}(n)\right] \cdot [H_{34}(n,a)] - [E_{34}(n,a)]\right)^{-1} \\ &\quad \cdot \left([E_{12}(n,a)] - \left[Z^{(a)}(n)\right] \cdot [H_{12}(n,a)]\right), \end{aligned} \tag{5}$$

$$[E_{pq}(n,r)] = \begin{bmatrix} \hat{\phi} \cdot \mathbf{e}^{(p)}_t(n,r) & \hat{\phi} \cdot \mathbf{e}^{(q)}_t(n,r) \\ \hat{z} \cdot \mathbf{e}^{(p)}_t(n,r) & \hat{z} \cdot \mathbf{e}^{(q)}_t(n,r) \end{bmatrix}, \tag{6}$$

$$[H_{pq}(n,r)] = \begin{bmatrix} \hat{\phi} \cdot \mathbf{h}^{(p)}_t(n,r) & \hat{\phi} \cdot \mathbf{h}^{(q)}_t(n,r) \\ \hat{z} \cdot \mathbf{h}^{(p)}_t(n,r) & \hat{z} \cdot \mathbf{h}^{(q)}_t(n,r) \end{bmatrix}, \tag{7}$$

$\hat{\phi}$, $\hat{z}$ being, respectively, the ϕ- and z-directed unit vectors.

2.2 Exact IBCs for an Inhomogeneous Dielectric Layer on a Cylinder

Let us next consider plane-wave incidence on a circular cylindrical surface at $r = a$ in the (r, ϕ, z) coordinate system, described by given IBCs and coated by an arbitrary isotropic but radially inhomogeneous (possibly lossy) dielectric layer, as depicted in Fig. 1. The relative permittivity profile $\epsilon_r(r)$ is assumed to be analytic [1] in $0 \le r \le b$, and, without loss in generality, monotonically decreasing. Also in this case the analysis is restricted to the case where the incident wave vector is orthogonal to the z axis (normal incidence). Again, the tangential

[1] This assumption, apparently unnecessary in the region $0 \le r \le a$, is actually required by the Frobenius technique used in the following. We stress that, even though the analytic permittivity profile is usually assigned only in the region $a \le r \le b$, this assumption does not hide any restriction or ambiguity, since one can always construct its (unique) analytical continuation (e.g., by means of Weiestrass procedure) in the region $0 \le r \le a$.

fields inside the coating can be expressed as Fourier series:

$$\begin{cases} \mathbf{E}_t(r,\phi) = \sum_{n=-\infty}^{\infty} \hat{\mathbf{E}}_t(n,r)\exp(in\phi), \\ \mathbf{H}_t(r,\phi) = \sum_{n=-\infty}^{\infty} \hat{\mathbf{H}}_t(n,r)\exp(in\phi). \end{cases} \tag{8}$$

Substituting the above in Maxwell equations readily gives [28]:

$$\frac{\partial^2 \hat{E}_z(n,r)}{\partial r^2} + \frac{1}{r}\frac{\partial^2 \hat{E}_z(n,r)}{\partial r} + \frac{q(n,r)}{r^2}\hat{E}_z(n,r) = 0, \tag{9}$$

$$\frac{\partial^2 \hat{H}_z(n,r)}{\partial r^2} + \frac{p(r)}{r}\frac{\partial^2 \hat{H}_z(n,r)}{\partial r} + \frac{q(n,r)}{r^2}\hat{H}_z(n,r) = 0, \tag{10}$$

which should be solved under the boundary conditions (3). In eqs. (9), (10):

$$q(n,r) = k_0^2 \mu_r \epsilon_r(r) r^2 - n^2, \tag{11}$$

and:

$$p(r) = 1 - \frac{r}{\epsilon_r(r)}\frac{d\epsilon_r(r)}{dr}, \tag{12}$$

$k_0 = 2\pi/\lambda_0$ being the free-space wavenumber, and μ_r the (constant) relative magnetic perrneability of the coating.

The remaining tangential field components can be written as [28]:

$$\hat{E}_\phi(n,r) = i\frac{\eta_0}{k_0\epsilon_r(r)}\frac{\partial \hat{H}_z(n,r)}{\partial r}, \tag{13}$$

$$\hat{H}_\phi(n,r) = -\frac{i}{k_0\eta_0\mu_r}\frac{\partial \hat{E}_z(n,r)}{\partial r}. \tag{14}$$

Eqs. (9), (10) belong to the general class of Sturm-Liouville problems [26]. Moreover, in view of the assumed analyticity of $\epsilon_r(r)$ and since $\epsilon_r(0) \neq 0$, the point $r = 0$ is recognized to be a *regular singular point* according to Fuchs classification [26], so that, as shown by Frobenius [26], eqs. (9), (10) admit solutions of the form:

$$\psi(r) = r^\alpha A(r), \quad \text{or} \quad \psi(r) = r^\alpha A(r)\log(r) + r^\beta B(r), \tag{15}$$

where $A(r)$, $B(r)$ are analytic at $r = 0$, and can be thus represented by Taylor expansions converging in a circle of the complex r-plane of

radius at least as large as the distance to the nearest singularity of $p(r)$ or $q(n,r)$ [26].

In the following, we shall sketch the Frobenius procedure [26] for solving eq. (10), since eq. (9) can be viewed as a particular case thereof ($p(r)=1$). Eq. (10) admits two independent solutions, say $h_z^{(1)}$, $h_z^{(2)}$, one of which is always an ordinary Frobenius expansion [26]:

$$h_z^{(1)}(n,r) = \psi(\alpha_1, r) := \sum_{j=0}^{\infty} a_j(\alpha_1)(k_0 r)^{\alpha_1 + j}, \tag{16}$$

α_1 being the *largest* solution of the *indicial equation* [26]

$$P(\alpha) := \alpha^2 + [p(0) - 1]\alpha + q(n,0) = \alpha^2 - n^2 = 0. \tag{17}$$

Without loss in generality, in the following we shall assume $n \geq 0$, so that $\alpha_1 = n$, $\alpha_2 = -n$. The a_j coefficients in (16) can be computed by using the Taylor expansions

$$p(r) = \sum_{j=0}^{\infty} p_j (k_0 r)^j, \tag{18}$$

$$q(n,r) = \sum_{j=0}^{\infty} q_j(n)(k_0 r)^j, \tag{19}$$

in eq. (10), and zeroing all coefficients of the same powers in $k_0 r$, whence [26],

$$\begin{cases} a_0(\alpha) = 1, \\ a_j(\alpha) = -\dfrac{\displaystyle\sum_{k=0}^{j-1} [(k+\alpha)p_{j-k} + q_{j-k}(n)]\, a_k(\alpha)}{P(j+\alpha)}, \quad j \geq 1. \end{cases} \tag{20}$$

It is readily verified that in the special case of a homogeneous profile the above expression reproduces, but for a multiplicative factor [2], the n-th order Bessel functions of the first kind [29].

[2] Different choices for the (arbitrary) value of a_0 affects the solution only by an overall multiplicative factor.

Computation of the second independent solution requires a different route, depending on whether $n = 0,\ 2n \in \aleph^+$ or otherwise [26]. In view of further developments, we need to discuss all three cases.

If $n = 0$, the second independent solution can be written as [26]:

$$h_z^{(2)}(0,r) = \frac{\partial}{\partial\alpha}\psi(\alpha,r)\bigg|_{\alpha=0} = h_z^{(1)}(0,r)\log(r) + \sum_{j=1}^{\infty}\tilde{a}_j(n)|_{n=0}(k_0 r)^j, \tag{21}$$

where

$$\begin{cases} \tilde{a}_0(n) = 0, \\ \tilde{a}_j(n) = -\dfrac{\displaystyle\sum_{k=0}^{j-1}\{p_{j-k}a_k(n) + [(n+k)p_{j-k} + q_{j-k}]\tilde{a}_k(n)\}}{P(j+n)} \\ \qquad\qquad + \dfrac{\displaystyle 4n\sum_{k=0}^{j-1}[(n+k)p_{j-k} + q_{j-k}]a_k(n)}{P^2(j+n)}, \quad j \geq 1, \end{cases} \tag{22}$$

the coefficients a_j being given by (20).

If $2n \in \aleph^+$ the second independent solution can be written as [3] [26]

$$\begin{aligned} h_z^{(2)}(n,r) &= \sum_{j=0}^{\infty} b_j(n)(k_0 r)^{j-n} - \gamma\,\frac{\partial}{\partial\alpha}\psi(\alpha,r)\bigg|_{\alpha=n} \\ &= \sum_{j=0}^{\infty} b_j(n)(k_0 r)^{j-n} - \gamma\sum_{j=1}^{\infty}\tilde{a}_j(n)(k_0 r)^{j+n}, \end{aligned} \tag{23}$$

where:

$$\begin{cases} b_0(n) = 1, \quad b_{2n}(n) = 0, \\ b_j(n) = -\dfrac{\displaystyle\sum_{k=0}^{j-2}[(k-n)p_{j-k} + q_{j-k}]b_k(n)}{P(j-n)}, \quad j \neq 0, 2n, \end{cases} \tag{24}$$

[3] In the (seldom occurring) special case where $\sum_{k=0}^{2n-1}[(k-n)p_{2n-k} + q_{2n-k}] = 0$, it can be shown that the second independent solution is again an ordinary Frobenius series of indicial exponent $\alpha_2 = -n$ [26].

$$\gamma = \frac{1}{P'(n)} \sum_{k=0}^{2n-1} [(k-n)p_{2n-k} + q_{2n-k}]b_k(n), \tag{25}$$

a prime indicates derivation with respect to the argument, and the coefficients $\tilde{a}_j$ are given by (22). If $2n \notin \aleph^+$, the second independent solution of (10) is again an ordinary Frobenius series with indicial exponent $\alpha_2 = -n$ [26].

Following the procedure outlined above, one can find the general solution of the Sturm-Liouville problems (9), (10), and hence the general expression for the tangential fields, viz.,

$$\begin{bmatrix} \hat{E}_\phi(n,r) \\ \hat{E}_z(n,r) \end{bmatrix} = [E_1(n,r)] \cdot \begin{bmatrix} A_n \\ C_n \end{bmatrix} + [E_2(n,r)] \cdot \begin{bmatrix} B_n \\ D_n \end{bmatrix}, \tag{26}$$

$$\begin{bmatrix} \hat{H}_\phi(n,r) \\ \hat{H}_z(n,r) \end{bmatrix} = [H_1(n,r)] \cdot \begin{bmatrix} A_n \\ C_n \end{bmatrix} + [H_2(n,r)] \cdot \begin{bmatrix} B_n \\ D_n \end{bmatrix}, \tag{27}$$

where $A_n,\ B_n,\ C_n,\ D_n$ are arbitrary constants and

$$[E_j(n,r)] = \begin{bmatrix} \dfrac{i\eta_0}{k_0\epsilon_r(r)} \dfrac{\partial h_z^{(j)}(n,r)}{\partial r} & 0 \\ 0 & e_z^{(j)}(n,r) \end{bmatrix}, \quad j = 1,2, \tag{28}$$

$$[H_j(n,r)] = \begin{bmatrix} 0 & -\dfrac{i}{k_0\eta_0\mu_r} \dfrac{\partial e_z^{(j)}(n,r)}{\partial r} \\ h_z^{(j)}(n,r) & 0 \end{bmatrix}, \quad j = 1,2, \tag{29}$$

$e_z^{(1)},\ e_z^{(2)}$ and $h_z^{(1)},\ h_z^{(2)}$ being two independent solutions of (9), (10), respectively. Again, for each value of n, the four unknown coefficients $A_n, \ldots, D_n$ can be successively eliminated by enforcing the known IBCs (3) at $r = a$ and the sought IBCs at $r = b$, yielding:

$$\begin{aligned} \left[Z^{(b)}(n)\right] = &\Big([E_1(n,b)] \cdot \left[Q^{(a)}(n)\right] + [E_2(n,b)]\Big) \\ &\cdot \Big([H_1(n,b)] \cdot \left[Q^{(a)}(n)\right] + [H_2(n,b)]\Big)^{-1}, \end{aligned} \tag{30}$$

where:

$$\begin{aligned} \left[Q^{(b)}(n)\right] = &\Big(\left[Z^{(a)}(n)\right] \cdot [H_1(n,b)] - [E_1(n,b)]\Big)^{-1} \\ &\cdot \Big([E_2(n,b)] - \left[Z^{(a)}(n)\right] \cdot [H_2(n,b)]\Big). \end{aligned} \tag{31}$$

By suitable iteration of the procedure outlined above a systematic derivation (for any value of the Fourier index n) of exact spectral domain IBCs for multi-layered circular cylindrical coatings consisting of an arbitrary number of stacked homogeneous bianisotropic and inhomogeneous dielectric layers is obtained.

3. SPATIAL DOMAIN HOIBCS ON A LOCALLY CYLINDRICAL SURFACE

Our ultimate goal consists in deriving spatial domain HOIBCs for *arbitrary* curved coatings which can be *locally* approximated by cylindrical surfaces. To this end, we use the discrete spectral information provided by the exact IBCs holding for all azimuthal harmonics in the cylindrical scattering case:

$$\begin{bmatrix} \hat{E}_\phi(n,b) \\ \hat{E}_z(n,b) \end{bmatrix} = \begin{bmatrix} Z^{(b)}_{\phi\phi}(n) & Z^{(b)}_{\phi z}(n) \\ Z^{(b)}_{z\phi}(n) & Z^{(b)}_{zz}(n) \end{bmatrix} \cdot \begin{bmatrix} \hat{H}_\phi(n,b) \\ \hat{H}_z(n,b) \end{bmatrix}, \tag{32}$$

to derive a spectral representation of the sought IBCs describing a general cylindrical surface, $r = b(\phi)$. One accordingly writes the sought IBCs as [7]:

$$\begin{bmatrix} \hat{E}_\ell(k_\ell b,b) \\ \hat{E}_z(k_\ell b,b) \end{bmatrix} = \begin{bmatrix} Z^{(b)}_{\ell\ell}(k_\ell b) & Z^{(b)}_{\ell z}(k_\ell b) \\ Z^{(b)}_{z\ell}(k_\ell b) & Z^{(b)}_{zz}(k_\ell b) \end{bmatrix} \cdot \begin{bmatrix} \hat{H}_\ell(k_\ell b,b) \\ \hat{H}_z(k_\ell b,b) \end{bmatrix}, \tag{33}$$

where $\hat{E}_\ell,\ \hat{E}_z,\ \hat{H}_\ell,\ \hat{H}_z$ are the (continuous, Fourier integral) spectral representation of the local tangential field components, viewed as functions of the *local* path-length $\ell = \int b(\phi) d\phi$. The matrix impedance components are accordingly formally obtained from the corresponding ones in (32) letting $k_\ell b$ in place of n, k_ℓ thus representing an azimuthal wavenumber, and b being the local curvature radius. Hoppe and Rahmat-Samii [7] suggested that the above IBCs can be viewed as *continuous* functions of k_ℓ and be conveniently approximated in terms of polynomials in k_ℓ, i.e,

$$\begin{bmatrix} P_1(k_\ell) & P_2(k_\ell) \\ P_3(k_\ell) & P_4(k_\ell) \end{bmatrix} \begin{bmatrix} \hat{E}_\ell(k_\ell b,b) \\ \hat{E}_z(k_\ell b,b) \end{bmatrix} \approx \begin{bmatrix} P_5(k_\ell) & P_6(k_\ell) \\ P_7(k_\ell) & P_8(k_\ell) \end{bmatrix} \begin{bmatrix} \hat{H}_\ell(k_\ell b,b) \\ \hat{H}_z(k_\ell b,b) \end{bmatrix}, \tag{34}$$

or, equivalently,

$$\begin{bmatrix} P_1(k_\ell) & P_2(k_\ell) \\ P_3(k_\ell) & P_4(k_\ell) \end{bmatrix} \begin{bmatrix} Z^{(b)}_{\ell\ell}(k_\ell b) & Z^{(b)}_{\ell z}(k_\ell b) \\ Z^{(b)}_{z\ell}(k_\ell b) & Z^{(b)}_{zz}(k_\ell b) \end{bmatrix} \approx \begin{bmatrix} P_5(k_\ell) & P_6(k_\ell) \\ P_7(k_\ell) & P_8(k_\ell) \end{bmatrix}, \tag{35}$$

where $P_1(k_\ell) - P_8(k_\ell)$ are polynomials in k_ℓ. Accordingly, the approximate spectral domain IBCs can be written as:

$$\begin{bmatrix} \tilde{Z}^{(b)}_{\ell\ell}(k_\ell b) & \tilde{Z}^{(b)}_{\ell z}(k_\ell b) \\ \tilde{Z}^{(b)}_{z\ell}(k_\ell b) & \tilde{Z}^{(b)}_{zz}(k_\ell b) \end{bmatrix} = \begin{bmatrix} P_1(k_\ell) & P_2(k_\ell) \\ P_3(k_\ell) & P_4(k_\ell) \end{bmatrix}^{-1} \cdot \begin{bmatrix} P_5(k_\ell) & P_6(k_\ell) \\ P_7(k_\ell) & P_8(k_\ell) \end{bmatrix}. \tag{36}$$

In the above expression each impedance term is approximated by a rational function of k_ℓ. In the following, we shall focus our attention on the second order case, i.e.,

$$P_j(k_\ell) = c_0^{(j)} + c_1^{(j)} k_\ell + c_2^{(j)} k_\ell^2, \quad j = 1, \ldots, 8, \tag{37}$$

where the unknown coefficients are usually computed via point-matching [7]. For the case of azimuthally isotropic coatings, relevant for all examples presented in the following, the linear terms in k_ℓ in (37) do not appear on account of the 180-deg symmetry [7]. In addition, it is always possible to let [7]:

$$c_0^{(1)} = c_0^{(4)} = 1, \quad c_0^{(2)} = c_0^{(3)} = 0. \tag{38}$$

The remaining twelve unknown coefficients in (37) can be computed by enforcing eq. (35) at normal incidence ($k_\ell = 0$) and at two distinct values of k_ℓ (usually $k_\ell^{(1)} = k_0/2$ and $k_\ell^{(2)} = k_0$, so as to span the whole visible range), as proposed in [7]. The complete solution is reported in Appendix A.

Once the coefficients are computed, the obtained polynomial approximation can be readily Fourier transformed into the spatial domain ($k_\ell \to id/d_\ell$), yielding the sought HOIBCs relating the ℓ and z field components, viz.,

$$\begin{aligned} &\left(1 - c_2^{(1)} \frac{d^2}{d\ell^2}\right) E_\ell(\ell) - c_2^{(2)} \frac{d^2 E_z(\ell)}{d\ell^2} \\ &= \left(c_0^{(5)} - c_2^{(5)} \frac{d^2}{d\ell^2}\right) H_\ell(\ell) + \left(c_0^{(6)} - c_2^{(6)} \frac{d^2}{d\ell^2}\right) H_z(\ell) \end{aligned} \tag{39}$$

and

$$
\begin{aligned}
&- c_2^{(3)} \frac{d^2 E_\ell(\ell)}{d\ell^2} + \left(1 - c_2^{(4)} \frac{d^2}{d\ell^2}\right) E_z(\ell) \\
&= - \left(c_0^{(6)} + c_2^{(7)} \frac{d^2}{d\ell^2}\right) H_\ell(\ell) + \left(c_0^{(5)} - c_2^{(8)} \frac{d^2}{d\ell^2}\right) H_z(\ell), \qquad (40)
\end{aligned}
$$

which are appropriate to describe a locally cylindrical coated scatterer with local curvature radius b.

4. APPLICATION EXAMPLES

Before dealing with application examples of the proposed HOIBCs, we briefly discuss the convergence features of the series involved in the proposed Frobenius solutions, since their evaluation is both required for the point-matching procedure and, obviously, for computing a benchmark solution. As seen from (30)–(31), one needs to evaluate these expansions at $r = a, b$, and thus, from a theoretic viewpoint the convergence is *always* assured, since $p(r)$, $q(n, r)$ are analytic in $a \leq r \leq b$. From a computational viewpoint, however, it is expected that the numerical convergence gets poorer and poorer as the local curvature radius of the coating increases. Actually, this does not represent a serious limitation[4], since for large (local) curvature radii the simpler HOIBCs relying on the locally planar approximation [7, 23] work quite well, and the improvement provided by the proposed HOIBCs is usually slight. As a matter of fact, in our numerical simulations we found that in the most interesting range $b \leq \lambda_0$, where the curvature effects are actually *non-negligible*, the convergence is quite good (five-digit accuracy with 200 terms, on average).

As a first example, we consider a two-layer coating consisting of a linear-profile inhomogeneous dielectric layer superimposed on a homogeneous chiral layer, laid on a perfectly conducting circular cylinder, as depicted in Fig. 2. The whole structure is assumed lossless, in order to get a more severe test. As well known, a chiral medium is described by the following constitutive relations [30, 31]:

$$
\begin{cases}
\mathbf{D} = \epsilon_0 \epsilon_r \mathbf{E} - i\gamma_c \mathbf{B}, \\
\mathbf{H} = \dfrac{1}{\mu_0 \mu_r} \mathbf{B} - i\gamma_c \mathbf{E},
\end{cases} \qquad (41)
$$

[4] However, standard methods commonly used for summing poorly convergent series (Shank's transformation, Padé approximation [26]) could be applied.

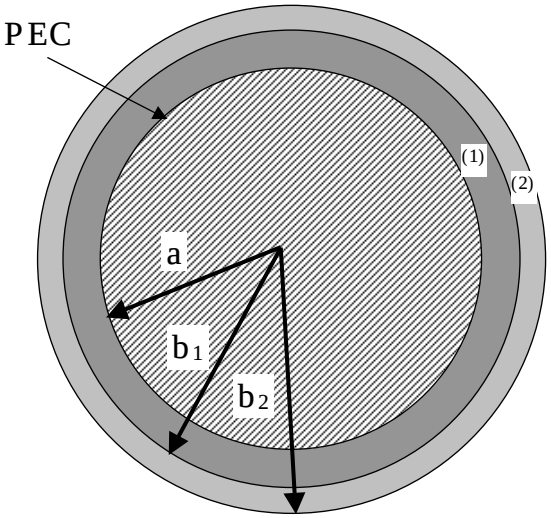

Figure 2. Two-layer coated cylinder. Layer 1: chiral medium ($\epsilon_{rc} = 3,\ \mu_r = 1,\ \gamma_c = 0.003\,\Omega^{-1}$); Layer 2: linear-profile dielectric ($\epsilon_{r1} = 3,\ \epsilon_{r2} = 2,\ \mu_r = 1$).

γ_c being the *chiral admittance*. The pertinent tangential characteristic cylindrical waves are reported in Appendix B. The inhomogeneous dielectric layer is described by the following profile:

$$\epsilon_r(r) = \epsilon_{r1} + \frac{r - b_1}{b_2 - b_1}(\epsilon_{r2} - \epsilon_{r1}), \quad b_1 \leq r \leq b_2. \tag{42}$$

HOIBCs at $r = b_2$ are obtained by using the procedures described in Sections 2, 3. In Figs. 3 and 4 the exact and second-order IBCs (locally planar [7, 23] and cylindrical approximation) are compared, as functions of the scaled azimuthal wavenumber. It is seen that for relatively thick cylinders ($b_2 = \lambda_0$, Fig. 3) the locally planar approximation, though less accurate, is still acceptable. For thinner cylinders ($b_2 = 0.42\lambda_0$, Fig. 4), on the other hand, locally planar approximation entails, as expected, large errors, while our solution provides a uniformly high accuracy.

In order to further elucidate this point, with reference to some physically meaningful measurable quantity, we compute the bistatic *echo width* [32], for plane-wave incidence from the $\phi = 0$ direction, viz.:

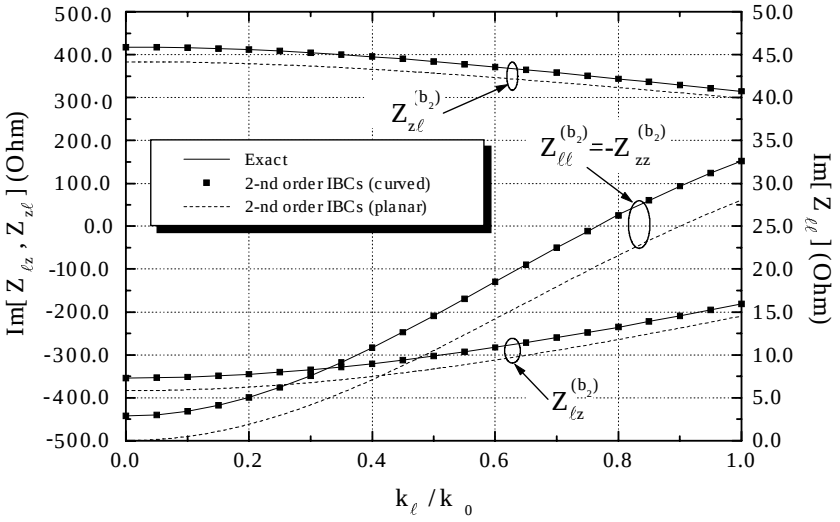

Figure 3. Comparison between exact and 2-nd order (planar and curved) IBCs for the two-layer coated cylinder of Fig. 2 ($a = 0.9\lambda_0$, $b_1 = 0.95\lambda_0$, $b_2 = \lambda_0$).

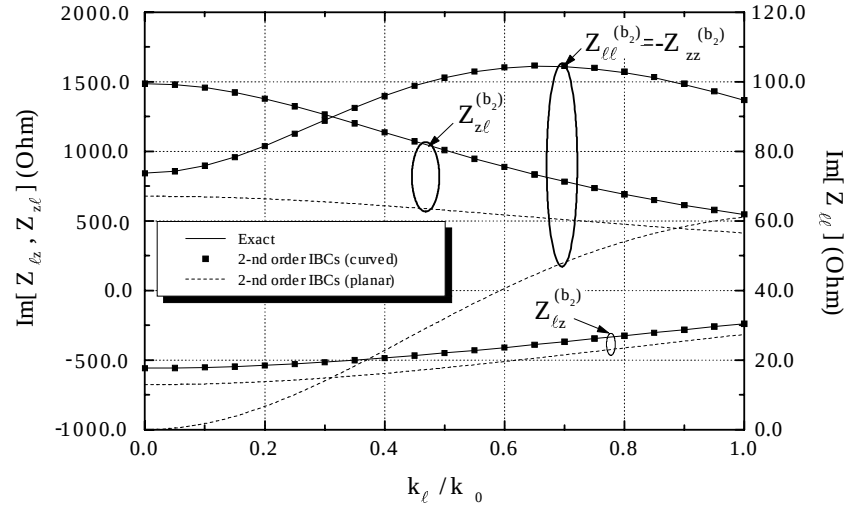

Figure 4. Comparison between exact and 2-nd order (planar and curved) IBCs for the two-layer coated cylinder of Fig. 2 ($a = 0.3\lambda_0$, $b_1 = 0.36\lambda_0, b_2 = 042\lambda_0$).

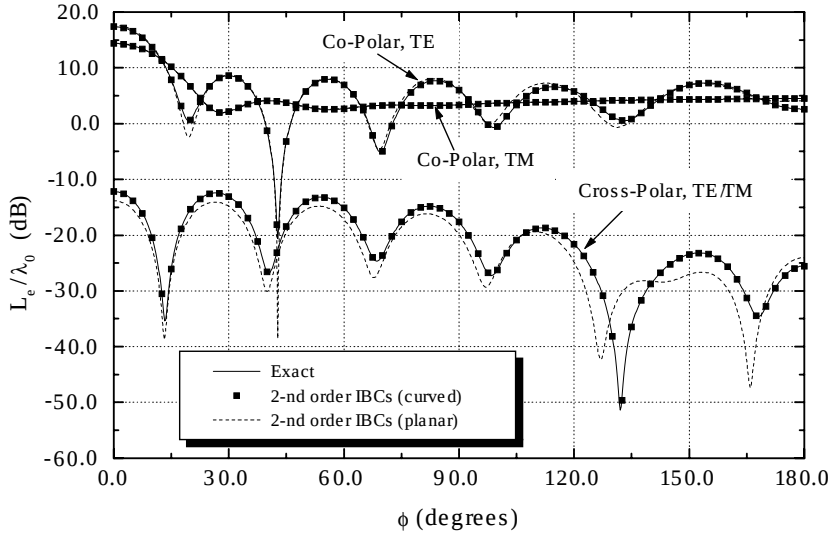

Figure 5. Bistatic echo width for the two-layer coated cylinder of Fig. 2 ($a = 0.9\lambda_0,\ b_1 = 0.95\lambda_0,\ b_2 = \lambda$).

$$L_e := \lim_{r\to\infty} \left(2\pi r \left| \frac{E^s}{E^i} \right|^2 \right), \tag{43}$$

$E^s,\ E^i$ being, respectively, the scattered and incident field.

The (co-polar TE and TM, as well as TE/TM cross-polar [5]) bistatic echo widths [6] for the same scatterers to which Figs. 3, 4 refer, are shown in Figs. 5 and 6, confirming the qualitative conclusions drawn from Figs. 3, 4. Remarkably, the proposed second-order IBCs are capable to model accurately the behavior of even smaller cylinders as exemplified in Fig. 7 ($b_2 = 0.1\lambda_0$). This suggests that they could be useful to model coated scatterers with (rounded) corners.

It is worth stressing that IBCs relying on normal incidence (i.e., $k_\ell = 0$), like Leontovich IBC and Tensor IBC [7], would fail in predicting *any* cross-polarized component of the reflected field.

[5] Note that cross-polarized components for TE and TM incidence are the same, as dictated by reciprocity.

[6] As well known, an exact analytical solution for circular cylinders can be obtained in terms of Fourier series involving Bessel/Hankel functions and surface impedances [7, 32].

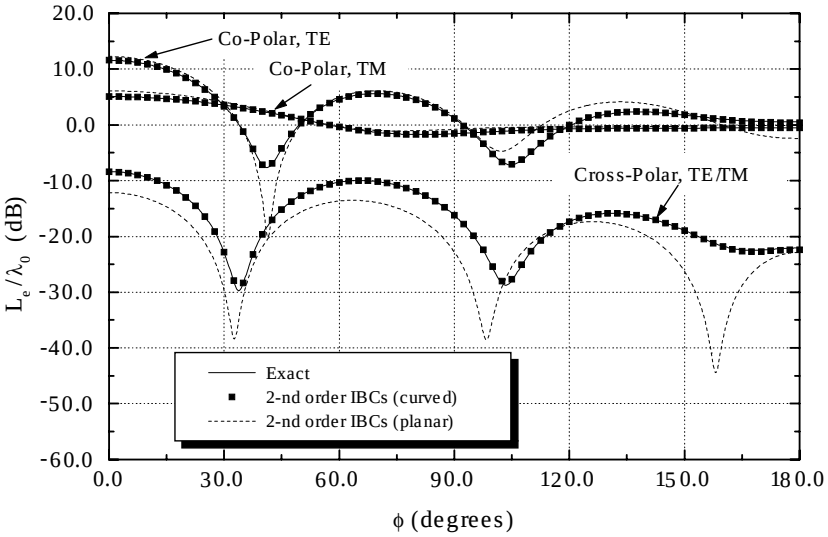

Figure 6. Bistatic echo width for the two-layer coated cylinder of Fig. 2 ($a = 0.3\lambda_0,\ b_1 = 0.36\lambda_0, b_2 = 0.42\lambda_0$).

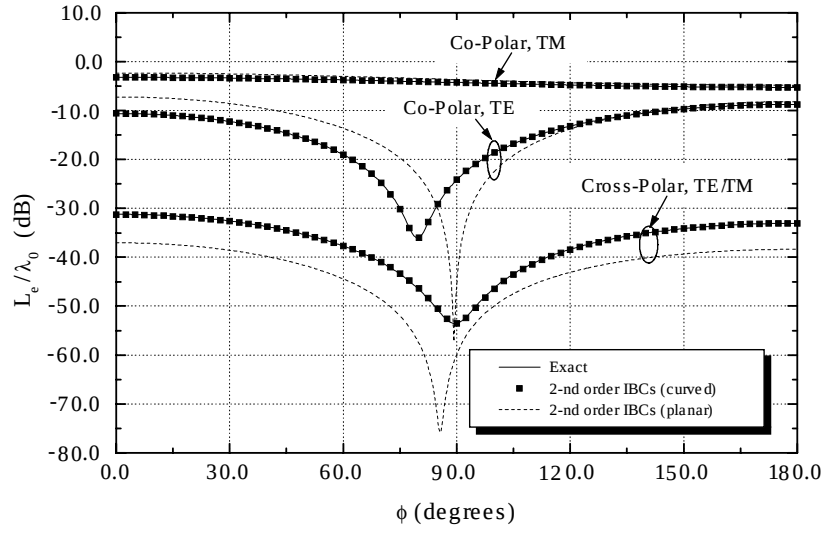

Figure 7. Bistatic echo width for the two-layer coated cylinder of Fig. 2 ($a = 0.05\lambda_0,\ b_1 = 0.075\lambda_0,\ b_2 = 0.1\lambda_0$).

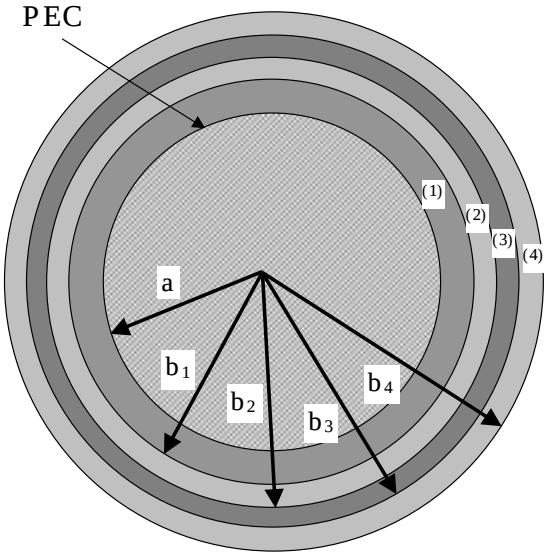

Figure 8. Four-layer coated cylinder. Layer 1: chiral medium ($\epsilon_{rc} = 4,\ \mu_r = 1,\ \gamma_c = 0.005\,\Omega^{-1}$); Layer 2: parabolic-profile dielectric ($\epsilon_{r1} = 4,\ \epsilon_{r2} = 3,\ \mu_r = 1$); Layer 3: bianisotropic medium ($\epsilon_{rb} = 3,\ \mu_r = 1,\ \xi = 0.3$); Layer 4: linear- profile dielectric ($\epsilon_{r3} = 3,\ \epsilon_{r4} = 2,\ \mu_r = 1$).

As a final example, we consider a fairly complex (lossless) four-layer coating, as sketched in Fig. 8. The bianisotropic layer is described by the following constitutive tensors:

$$\overline{\epsilon} = \epsilon_{rb}\overline{I}, \quad \overline{\mu} = \mu_r\overline{I}, \quad \overline{\xi} = \overline{\zeta} = \begin{bmatrix} 0 & i\xi & 0 \\ -i\xi & 0 & 0 \\ 0 & 0 & 0 \end{bmatrix}, \tag{44}$$

$\overline{I}$ being the identity matrix. Although likely unphysical, this is an example of material for which TE-TM decoupling occurs (see Appendix C for the pertinent characteristic cylindrical waves).

The inner inhomogeneous dielectric layer is described by the following parabolic profile

$$\epsilon_r(r) = \epsilon_{r1} + \frac{\left(r^2 - b_1^2\right)}{\left(b_2^2 - b_1^2\right)}\left(\epsilon_{r2} - \epsilon_{r1}\right), \quad b_1 \le r \le b_2. \tag{45}$$

In Figs. 9, 10 the bistatic echo widths, computed using exact and second-order IBCs, for different values of the geometric parameters,

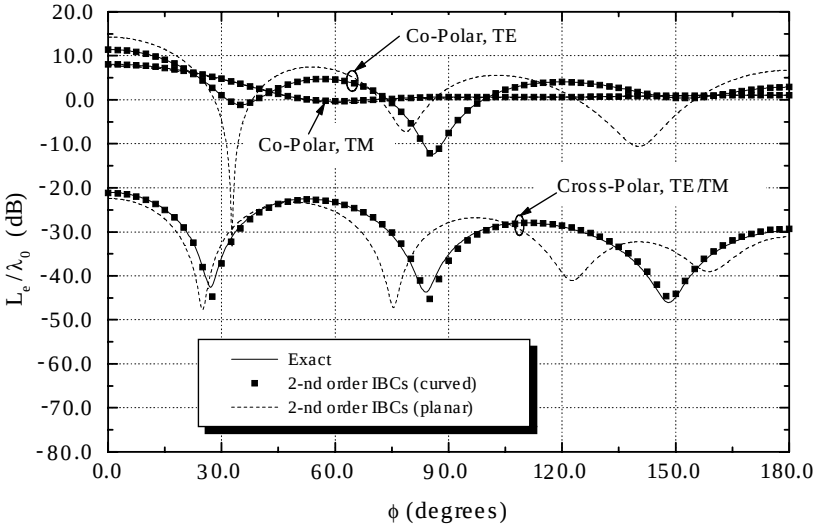

Figure 9. Bistatic echo width for the four-layer coated cylinder of Fig. 8 ($a = 0.4\lambda_0,\ b_1 = 0.425\lambda_0,\ b_2 = 0.45\lambda_0,\ b_3 = 0.475\lambda_0,\ b_4 = 0.5\lambda_0$) .

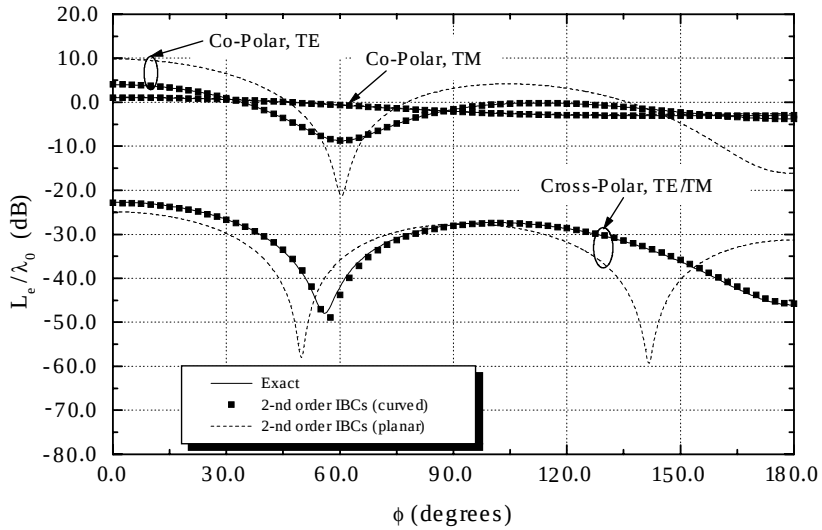

Figure 10. Bistatic echo width for the four-layer coated cylinder of Fig. 8 ($a = 0.12\lambda_0,\ b_1 = 0.14\lambda_0,\ b_2 = 0.16\lambda_0,\ b_3 = 0.18\lambda_0,\ b_4 = 0.2\lambda_0$).

are displayed. Again, the excellent accuracy provided by the proposed second-order IBCs is evident, whereas locally planar approximation gives fairly poorer results.

5. CONCLUSIONS

We presented a systematic SDRA approach for deriving HOIBCs describing stratified coatings consisting of homogeneous bianisotropic and inhomogeneous dielectric layers laid on conducting cylinders. The proposed method enables for accounting one-dimensional curvature effects, by extending the approach formulated by Hoppe and Rahmat-Samii for homogeneous coatings [7].

Application examples, involving fairly complex multi-layer coatings and second-order IBCs, validate the proposed approach and demonstrate its improved accuracy with respect to locally planar approximation, as far as local curvature radii smaller than a free-space wavelength are concerned.

It is argued that the proposed HOIBCs could be profitably applied to locally cylindrical surfaces, where, e.g., only one of the two local principal curvature radii is large in terms of a wavelength.

A more or less straightforward extension involves the analysis of oblique incidence. Extension to the case where both local principal radii are comparable to a wavelength, though conceptually similar, leads to a less handy canonical problem.

APPENDIX A. DETERMINATION OF COEFFICIENTS IN EQ. (37)

By enforcing eq. (35) at $k_\ell = 0,\ k_\ell^{(1)},\ k_\ell^{(2)}$ one gets [7]:

$$c_0^{(5)} = Z_{\ell\ell}^{(b)}(0), \quad c_0^{(6)} = Z_{\ell z}^{(b)}(0), \quad c_0^{(7)} = Z_{z\ell}^{(b)}(0), \quad c_0^{(8)} = Z_{zz}^{(b)}(0), \quad (46)$$

$$\begin{bmatrix} c_2^{(1)} \\ c_2^{(2)} \\ c_2^{(5)} \\ c_2^{(6)} \end{bmatrix} = [M]^{-1} \cdot \begin{bmatrix} Z_{\ell\ell}^{(b)}(0) - Z_{\ell\ell}^{(b)}(k_\ell^{(1)} b) \\ Z_{\ell z}^{(b)}(0) - Z_{\ell z}^{(b)}(k_\ell^{(1)} b) \\ Z_{\ell\ell}^{(b)}(0) - Z_{\ell\ell}^{(b)}(k_\ell^{(2)} b) \\ Z_{\ell z}^{(b)}(0) - Z_{\ell z}^{(b)}(k_\ell^{(2)} b) \end{bmatrix}, \quad (47)$$

$$\begin{bmatrix} c_2^{(3)} \\ c_2^{(4)} \\ c_2^{(7)} \\ c_2^{(8)} \end{bmatrix} = [M]^{-1} \cdot \begin{bmatrix} Z_{z\ell}^{(b)}(0) - Z_{z\ell}^{(b)}(k_\ell^{(1)} b) \\ Z_{zz}^{(b)}(0) - Z_{zz}^{(b)}(k_\ell^{(1)} b) \\ Z_{z\ell}^{(b)}(0) - Z_{z\ell}^{(b)}(k_\ell^{(2)} b) \\ Z_{zz}^{(b)}(0) - Z_{zz}^{(b)}(k_\ell^{(2)} b) \end{bmatrix}, \tag{48}$$

where

$$[M] = \begin{bmatrix} {k_\ell^{(1)}}^2 Z_{\ell\ell}^{(b)}(k_\ell^{(1)}) & {k_\ell^{(1)}}^2 Z_{z\ell}^{(b)}(k_\ell^{(1)}) & -{k_\ell^{(1)}}^2 & 0 \\ {k_\ell^{(1)}}^2 Z_{\ell z}^{(b)}(k_\ell^{(1)}) & {k_\ell^{(1)}}^2 Z_{zz}^{(b)}(k_\ell^{(1)}) & 0 & -{k_\ell^{(1)}}^2 \\ {k_\ell^{(2)}}^2 Z_{\ell\ell}^{(b)}(k_\ell^{(2)}) & {k_\ell^{(2)}}^2 Z_{z\ell}^{(b)}(k_\ell^{(2)}) & -{k_\ell^{(2)}}^2 & 0 \\ {k_\ell^{(2)}}^2 Z_{\ell z}^{(b)}(k_\ell^{(2)}) & {k_\ell^{(2)}}^2 Z_{zz}^{(b)}(k_\ell^{(2)}) & 0 & -{k_\ell^{(2)}}^2 \end{bmatrix}. \tag{49}$$

APPENDIX B. CHARACTERISTIC CYLINDRICAL WAVES FOR A CHIRAL MEDIUM

For a chiral medium, the appropriate transverse characteristic cylindrical waves are the radially forward and backward propagating right-hand and left-hand circularly polarized cylindrical waves, viz. [27],

$$\mathbf{e}_t^{(1)}(n,r) = -J_n'(k_R r)\hat{\phi} + J_n(k_R r)\hat{z},\ \mathbf{h}_t^{(1)}(n,r) = \frac{i}{\eta_c}\mathbf{e}_t^{(1)}(n,r), \tag{50}$$

$$\mathbf{e}_t^{(2)}(n,r) = -H_n^{(2)\prime}(k_R r)\hat{\phi} + H_n^{(2)}(k_R r)\hat{z},\ \mathbf{h}_t^{(2)}(n,r) = \frac{i}{\eta_c}\mathbf{e}_t^{(2)}(n,r), \tag{51}$$

$$\mathbf{e}_t^{(3)}(n,r) = -J_n'(k_L r)\hat{\phi} - J_n(k_L r)\hat{z},\ \mathbf{h}_t^{(3)}(n,r) = -\frac{i}{\eta_c}\mathbf{e}_t^{(3)}(n,r), \tag{52}$$

$$\mathbf{e}_t^{(4)}(n,r) = -H_n^{(2)\prime}(k_L r)\hat{\phi} + H_n^{(2)}(k_L r)\hat{z},\ \mathbf{h}_t^{(4)}(n,r) = \frac{i}{\eta_c}\mathbf{e}_t^{(4)}(n,r), \tag{53}$$

where $J_n(\cdot)$, $H_n^{(2)}(\cdot)$ denote n-th order Bessel functions of the first kind, and Hankel functions of the second kind [7], respectively [29], and

$$\left.\begin{matrix} k_R \\ k_L \end{matrix}\right\} = k_0\sqrt{\mu_r\left(\epsilon_r + \mu_r\eta_0^2\gamma_c^2\right)} \pm k_0\eta_0\gamma_c, \quad \eta_c = \eta_0\sqrt{\frac{\mu_r}{\epsilon_r + \mu_r\eta_0^2\gamma_c^2}}. \tag{54}$$

[7] Note that, in the case of no (half-)integer values of $n = k_\ell/b$, one can use $J_{-n}(\cdot)$ in place of $H_n^{(2)}(\cdot)$.

APPENDIX C. CHARACTERISTIC CYLINDRICAL WAVES FOR THE BIANISOTROPIC MEDIUM DESCRIBED BY EQ. (44)

The bianisotropic material described by the constitutive relations (44) is a nice example of a medium where TE-TM decoupling in cylindrical coordinates occurs [25]. It is readily found that the longitudinal field components satisfy standard Bessel equation [25], and the transverse cylindrical waves can be accordingly written as follows:

$$\begin{cases} \mathbf{e}_t^{(1)}(n,r) = J_n(k_b r)\hat{z} + \dfrac{1}{k_b r\sqrt{\epsilon_{rb}\mu_r - \xi^2}} \\ \qquad\qquad \cdot \left[-in\xi J_n(k_b r) + i\mu_r k_b r J_n'(k_b r)\right]\hat{\phi}, \\ \mathbf{h}_t^{(1)}(n,r) = \dfrac{J_n(k_b r)}{\eta_0}\hat{z} + \dfrac{1}{\eta_0 k_b r\sqrt{\epsilon_{rb}\mu_r - \xi^2}} \\ \qquad\qquad \cdot \left[in\xi J_n(k_b r) - i\epsilon_{rb} k_b r J_n'(k_b r)\right]\hat{\phi}, \end{cases} \tag{55}$$

$$\begin{cases} \mathbf{e}_t^{(2)}(n,r) = H_n^{(2)}(k_b r)\hat{z} + \dfrac{1}{k_b r\sqrt{\epsilon_{rb}\mu_r - \xi^2}} \\ \qquad\qquad \cdot \left[-in\xi H_n^{(2)}(k_b r) + i\mu_r k_b r H_n^{(2)\prime}(k_b r)\right]\hat{\phi}, \\ \mathbf{h}_t^{(2)}(n,r) = \dfrac{H_n^{(2)}(k_b r)}{\eta_0}\hat{z} + \dfrac{1}{\eta_0 k_b r\sqrt{\epsilon_{rb}\mu_r - \xi^2}} \\ \qquad\qquad \cdot \left[in\xi H_n^{(2)}(k_b r) - i\epsilon_{rb} k_b r J_n'(k_b r)\right]\hat{\phi}, \end{cases} \tag{56}$$

$$\begin{cases} \mathbf{e}_t^{(3)}(n,r) = -J_n(k_b r)\hat{z} + \dfrac{1}{k_b r\sqrt{\epsilon_{rb}\mu_r - \xi^2}} \\ \qquad\qquad \cdot \left[in\xi J_n(k_b r) + i\mu_r k_b r J_n'(k_b r)\right]\hat{\phi}, \\ \mathbf{h}_t^{(3)}(n,r) = \dfrac{J_n(k_b r)}{\eta_0}\hat{z} + \dfrac{1}{\eta_0 k_b r\sqrt{\epsilon_{rb}\mu_r - \xi^2}} \\ \qquad\qquad \cdot \left[in\xi J_n(k_b r) + i\epsilon_{rb} k_b r J_n'(k_b r)\right]\hat{\phi}, \end{cases} \tag{57}$$

$$\begin{cases} \mathbf{e}_t^{(4)}(n,r) = -H_n^{(2)}(k_b r)\hat{z} + \dfrac{1}{k_b r\sqrt{\epsilon_{rb}\mu_r - \xi^2}} \\ \qquad\qquad \cdot \left[in\xi H_n^{(2)}(k_b r) + i\mu_r k_b r H_n^{(2)\prime}(k_b r)\right]\hat{\phi}, \\ \mathbf{h}_t^{(4)}(n,r) = \dfrac{H_n^{(2)}(k_b r)}{\eta_0}\hat{z} + \dfrac{1}{\eta_0 k_b r\sqrt{\epsilon_{rb}\mu_r - \xi^2}} \\ \qquad\qquad \cdot \left[in\xi H_n^{(2)}(k_b r) + i\epsilon_r k_b r H_n^{(2)\prime}(k_b r)\right]\hat{\phi}, \end{cases} \tag{58}$$

where

$$k_b = k_0\sqrt{\epsilon_{rb}\mu_r - \xi^2}. \tag{59}$$

REFERENCES

1. Strifors, H. C., and G. C. Gaunaurd, "Scattering of electromagnetic pulses by simple-shaped targets with radar cross section modified by a dielectric coating," *IEEE Trans. Antennas Propagat.,* Vol. 46, No. 9, 1252–1262, 1998.
2. Schulz, R. B., V. C. Plantz, and D. R. Brush, "Shielding theory and practice," *IEEE Trans. Electromag. Comp.,* Vol. 30, No. 3, 187–201, 1988.
3. Nishizawa, S., and O. Hashimoto, "Effectiveness analysis of lossy dielectric shields for a three-layered human model," *IEEE Trans. Microwave Theory Tech.,* Vol. 47, No. 3, 277–282, 1999.
4. Michielssen, E., J.-M. Sajer, S. Ranjithan, and R. Mittra, "Design of lightweight, broad-band microwave absorbers using genetic algorithms," *IEEE Trans. Microwave Theory Tech.,* Vol. 41, 1024–1031, 1993.
5. Norgren, M., and S. He, "On the possibility of reflectionless coating of a homogeneous bianisotropic layer on a perfect conductor," *Electromagnetics,* Vol. 17, 295–307, 1997.
6. Senior, T. B. A., and J. L. Volakis, *Approximate Boundary Conditions in Electromagnetics,* IEE Press, Stevenage, U.K., 1995.
7. Hoppe, D. J., and Y. Rahmat-Samii, *Impedance Boundary Conditions in Electromagnetics,* Taylor & Francis, Washington, 1995.
8. Harrington, R. F., *Field Computation by Moment Methods,* McMillan, New York, 1960.
9. Silvester, P. P., and R. L. Ferrari, *Finite Elements for Electrical Engineering,* Univ. Press, Cambridge, 1990.

10. Leontovich, M. A., *Investigations on Radiowave Propagation,* Part II, Academy of Sciences, Moskow, 1948.
11. Karp, S. N., and F. C. Karal, Jr., "Generalized impedance boundary conditions with application to surface wave structures," in *Electromagnetic Theory,* Part I, 479–483, Pergamon, New York, 1965.
12. Weinstein, A. L., *The Theory of Diffraction and the Factorization Method,* Golem, Boulder, Co., 1969.
13. Senior, T. B. A., and J. L. Volakis, "Derivation and application of a class of generalized impedance boundary conditions," *IEEE Trans. Antennas Propagat.,* Vol. 37, No. 12, 1566–1572, 1989.
14. Idemen, M., "Universal boundary conditions of the electromagnetic fields," *J. Phys. Soc. Jap.,* Vol. 59, No. 1, 71–80, 1990.
15. Volakis, J. L., and T. B. A. Senior, "Sheet simulation of a thin dielectric layer," *Radio Science,* Vol. 22, No. 7, 1261–1272, 1987.
16. Volakis, J. L., and T. B. A. Senior, "Application of a class of generalized boundary conditions to scattering by a metal-backed dielectric half-plane," *Proc. IEEE,* Vol. 77, No. 5, 796–805, 1989.
17. Ammari, H., and S. He, "Generalized effective impedance boundary conditions for an inhomogeneous thin layer in electromagnetic scattering," *J. Electromagn. Waves Applicat.,* Vol. 11, 1197–121, 1997.
18. Ammari, H., and S. He, "Effective impedance boundary conditions for an inhomogeneous thin layer on a curved metallic surface," *IEEE Trans. Antennas Propagat.,* Vol. 46, No. 5, 710–715, 1998.
19. Barkeshli, K., and J. L. Volakis, "TE scattering by a one-dimensional groove in a ground-plane using higher-order impedance boundary conditions," *IEEE Trans. Antennas Propagat.,* Vol. 38, No. 9, 1421–1428, 1990.
20. Volakis, J. L., and H. H. Syed, "Application of higher order boundary conditions to scattering by multilayer coated cylinders," *J. Electromagn. Waves Applicat.,* Vol. 4, No. 12, 1157–1180.
21. Ricoy, M. A., and J. L. Volakis, "Derivation of generalized transition/boundary conditions for planar multiple-layer structures," *Radio Science,* Vol. 25, No. 4, 391–405, 1990.
22. Tretyakov, S. A., "Generalized impedance boundary conditions for isotropic multilayers," *Microwave Opt. Technol. Lett.,* Vol. 17, No. 4, 262–265, 1998.

23. Galdi, V., and Pinto, I. M., "Derivation of higher-order impedance boundary conditions for stratified coatings composed of inhomogeneous-dielectric and/or homogeneous-bianisotropic layers," submitted to Radio Science, Feb. 1999.
24. Kong, J. A., *Theory of Electromagnetic Waves,* Wiley, New York, 1975.
25. Graglia, R. D., M. S. Sarto, and P. L. E. Uslenghi, "TE and TM modes in cylindrical metallic structures filled with bianisotropic material," *IEEE Trans. Microwave Theory Tech.,* Vol. 44, No. 8, 1470–1477, 1996.
26. Bender, C. M., and S. A. Orszag, *Advanced Mathematical Methods for Scientists and Engineers,* McGraw-Hill, New York, 1978.
27. Kluskens, M. S., and E. H. Newman, "Scattering by a multilayer chiral cylinder," *IEEE Trans. Antennas Propagat.,* Vol. 39, No. 1, 91–96, 1991.
28. Snyder, A. W., and J. D. Love, *Optical Waveguide Theory,* Chapman & Hall, London, U.K., 1983.
29. Abramowitz, M., and I. A. Stegun, *Handbook of Mathematical Functions,* Dover, New York, 1964.
30. Jaggard, D. L., A. R. Michelson, and C. H. Papas, "On electromagnetic waves in chiral media," *Appl. Phys.,* Vol. 118, 211–216, 1979.
31. Engheta, N., and D. L. Jaggard, "Electromagnetic chirality and its applications," *IEEE Antennas Propagat. Soc. Newsletter,* Vol. 30, No. 5, 6–12, 1988.
32. Harrington, R. F., *Time-Harmonic Electromagnetic Fields,* McGraw-Hill, New York, 1961.